nature communications

Article

https://doi.org/10.1038/s41467-024-52945-8

AtPRMT3-RPS2B promotes ribosome biogenesis and coordinates growth and cold adaptation trade-off

Received: 21 December 2023

Accepted: 25 September 2024

Published online: 08 October 2024

Check for updates

Zhen Wang[1,2,3,4] ✉, Xiaofan Zhang[1,2,4], Chunyan Liu[1], Susan Duncan[3], Runlai Hang[1], Jing Sun[1], Lilan Luo[1], Yiliang Ding[3] & Xiaofeng Cao[1,2] ✉

Translation, a fundamental process regulating cellular growth and proliferation, relies on functional ribosomes. As sessile organisms, plants have evolved adaptive strategies to maintain a delicate balance between growth and stress response. But the underlying mechanisms, particularly on the translational level, remain less understood. In this study, we revealed the mechanisms of AtPRMT3-RPS2B in orchestrating ribosome assembly and managing translational regulation. Through a forward genetic screen, we identified *PDCD2-D1* as a suppressor gene restoring abnormal development and ribosome biogenesis in *atprmt3-2* mutants. Our findings confirmed that PDCD2 interacts with AtPRMT3-RPS2B, and facilitates pre-ribosome transport through nuclear pore complex, finally ensuring normal ribosome translation in the cytoplasm. Additionally, the dysfunction of AtPRMT3-RPS2B was found to enhance freezing tolerance. Moreover, we revealed that AtPRMT3-RPS2B promotes the translation of housekeeping mRNAs while concurrently repressing stress-related mRNAs. In summary, our study sheds light on the regulatory roles of AtPRMT3-RPS2B in ribosome assembly and translational balance, enabling the trade-off between growth and stress.

Low temperature represents a major environmental factor limiting plant growth and development. Due to their sessile nature, plants have evolved sophisticated mechanisms to cope with stress conditions[1,2]. For instance, cold acclimation is a phenomenon wherein plants increase freezing tolerance after exposure to low non-freezing temperatures[3]. Researches over the past decades have unveiled extensive networks of the transcriptional and post-translational regulation of cold signaling pathways[4]. However, how translational regulation is involved in this adaptive process remains less characterized.

Ribosomes are essential for protein synthesis, making them vital for cell proliferation and survival. Ribosome biogenesis is one of the most intricate and energy-consuming programs in a cell. This process originates with ribosomal DNA (rDNA) transcription in the nucleolus, and then the precursor rRNAs (pre-rRNAs) will undergo processing, modification, and assembly process to form a large ribonucleoprotein complex termed 90S pre-ribosome, assisted by multiple assembly factors[5–7]. Subsequently, the 90S pre-ribosome complex splits into precursors of the 40S and 60S (pre-40S and pre-60S) particles, and undergo independent maturation steps[5,6]. The nuclear pore complex (NPC) serves as a central role in ribosome biogenesis by facilitating the transport of pre-ribosomal particles from the nucleus to the cytoplasm, where they undergo further processing to assemble into functional ribosomes[8,9]. The NPC is a sophisticated cellular structure embedded in the nuclear envelope, facilitating the exchange of molecules between the nucleus and the cytoplasm. Disruptions in nucleocytoplasmic transport have profound consequences on cellular function and stress responses[10–12].

[1]Institute of Genetics and Developmental Biology, Chinese Academy of Sciences, Beijing, China. [2]University of Chinese Academy of Sciences, Beijing, China. [3]John Innes Centre, Norwich Research Park, Norwich, United Kingdom. [4]These authors contributed equally: Zhen Wang, Xiaofan Zhang.
✉e-mail: z.wang@genetics.ac.cn; xfcao@genetics.ac.cn

Ribosome biogenesis and translation dynamics are tightly orchestrated during developmental programs and various stress responses, ensuring optimal growth adaptation[13–18]. This process is stringently regulated during environmental changes to ensure efficient ribosome activity[19]. During stress conditions, plants usually sacrifice their growth in order to better survive, generally, there is a balance between active growth and stress-responsive gene expression[17,20]. The translational regulation of stress-growth trade-off represents an efficient strategy. In yeast, the translation initiation factor Ded1p acts as a translational switch between housekeeping and stress mRNAs[21]. Similarly, in *Arabidopsis*, the defects of DHH1/DDX6-like proteins RNA HELICASE, RH6/8/12, could shift growth and stress transcriptome and translatome homeostasis[22]. AtPRMT3, a family of protein arginine methyltransferase, actively participates in ribosome biogenesis[23]. Its interaction with ribosomal protein RPS2B is crucial for regulating pre-ribosome biogenesis in the nucleus, thereby repressing nucleolus stress[24]. However, its underlying mechanisms in regulating ribosome biogenesis as well as the broader implications for plant growth and stress response regulation still require further elucidation.

In this study, we conducted a forward genetic screen and isolated a dominant suppressor, named *atprmt3pdcd2-d1*, which partially rescued the developmental defects and aberrant ribosome biogenesis in *atprmt3-2* mutants. Our findings established the involvement of PDCD2 in AtPRMT3-RPS2B mediated ribosome biogenesis. We demonstrated that PDCD2 could regulate the pre-ribosome biogenesis in the nucleus by promoting their efficient export to cytoplasm. Additionally, we identified that AtPRMT3-RPS2B was a negative regulator in freezing stress. We employed polysome profile combined with Ribo-seq to illustrate that AtPRMT3-RPS2B maintains gene translational balance. The disruption of *AtPRMT3-RPS2B* enhances the translation of specific mRNA linked to cold stress, thereby conferring freezing tolerant phenotype. Above all, we demonstrate a regulatory mechanism of AtPRMT3-RPS2-PDCD2 in ribosome biogenesis and translational trade-off between stress tolerance and normal growth.

Results

Mutation in *PDCD2* is responsible for suppressor of *atprmt3* mutants

AtPRMT3 is crucial for pre-ribosome assembly, and the defects of AtPRMT3 lead to pleiotropic developmental defects[23,24]. To gain deeper insights into the underlying mechanisms, we performed a forward genetic screen to identify the suppressors of *atprmt3* mutants. Notably, we isolated a suppressor named *m20*, partially rescued the developmental defects observed in *atprmt3* mutants. This rescue was evident in delayed growth state (Supplementary Fig. 1a), restored leaf morphology, including the pointed first leaves and disrupted leaf vein patterns (Supplementary Fig. 1b), and recovery of short primary root (Supplementary Fig. 1c, d).

Genetic analysis showed that *m20* represented a semi-dominant mutation in a single nuclear gene (Supplementary Fig. 1e). To pinpoint the causal gene mutation in *m20*, we performed whole-genome re-sequencing and mapped to At4g02220, which contains a G-to-A mutation in its 9th exon, and converts Glutamicacid-350 into Lysine (E350K) (Supplementary Fig. 1f). At4g02220 encodes a protein characterized by a zinc finger (MYND type) domain and a programmed cell death 2 C-terminal domain (Supplementary Fig. 1g), which is conserved and widely existed across different species (Supplementary Fig. 2a). PDCD2 has localization in both cytoplasm and nucleus (Supplementary Fig. 2b). Next, we expressed *ProUBQ10:PDCD2^{E350K}-HA* in *atprmt3-2* mutants, finding that the transgenic plants *PDCD2^{E350K}-HA* partially rescued the developmental defects of *atprmt3-2* mutants (Fig. 1a–d). The above genetic results demonstrated that *PDCD2^{E350K}* was responsible for the rescued phenotype in *m20*, hereafter, we renamed *m20* as *atprmt3pdcd2-d1*. Additionally, we used CRISPR-Cas9 to knock out *PDCD2*, and got two weak alleles of *pdcd2-cr1* (15-bp deletion) and *pdcd2-cr2* (12-bp deletion) (Supplementary Fig. 1h). We observed that *pdcd2-cr* mutants as well as *pdcd2-d1* single mutants exhibit no obvious developmental defects (Supplementary Fig. 1i).

Mutation in *PDCD2* rescues the aberrant ribosome biogenesis in *atprmt3* mutants

Then we wondered whether the suppressor could restore the aberrant pre-rRNA processing of *atprmt3* mutants. We performed Northern blot assay to determine the pre-rRNA state, rRNA processing intermediates could be detected by probes as previously described[23,24]. We observed that the defective pre-rRNA processing state was restored in suppressor *atprmt3pdcd2-d1* as probed by S7 and S9 (Fig. 1e). For example, probe S7 detected that the suppressor rescued the accumulated level of 33S(P')/32S and 18S-A3/A2 intermediates, and decreased level of P-A2/A3 intermediates in *atprmt3-2* mutants; probe S9 proved that the accumulated level of 33S(P')/32S, 27SA/27SB and pre-5.8S intermediates were also rescued in the suppressor (Fig. 1e).

During ribosome biogenesis, U3 small nucleolar ribonucleoprotein (snoRNP) is an essential component within the 90S/SSU processome, consisting of U3 snoRNA and core proteins, including Nucleolar protein 1 (NOP1)/FIBRILLARIN (FIB), NOP56, NOP58, Small nuclear protein 13 (Snu13), and RRP9[25]. We observed that the expression levels of *FIB1*, *FIB2*, *NOP56*, and *NOP58* were accumulated in *atprmt3-2* mutants, and they were restored in the suppressor *atprmt3pdcd2-d1* (Fig. 1f). Similarly, the accumulated U3 snoRNAs observed in the *atprmt3-2* mutants were also restored in the suppressor *atprmt3pdcd2-d1* (Fig. 1g). Similarly, we also assessed the rescued protein levels of FIB1 and NOP56 in the suppressor *atprmt3pdcd2-d1* (Fig. 1h). The above results indicate that *PDCD2-D1* mutation effectively rescues the aberrant ribosome biogenesis in *atprmt3-2* mutants.

PDCD2 is an interacting partner of AtPRMT3 and RPS2

PDCD2 features a MYND-type zinc finger domain (ZF-MYND) that facilitates protein-protein interactions. To ascertain the significance of ZF-MYND domain of PDCD2, we deleted the ZF-MYND domain in PDCD2^{E350K} to create *ProUBQ10:PDCD2$^{E350K\&\Delta ZF}$-HA*, and introduced into *atprmt3-2* mutants (Fig. 2a). The transgenic plants *PDCD2$^{E350K\&\Delta ZF}$-HA* could not rescue the developmental defects of *atprmt3-2* mutants (Fig. 2b, c, and Supplementary Fig. 3a), underscoring the essential function of ZF-MYND domain. We subsequently aimed to identify the interacting proteins of PDCD2 to uncover its biochemical functions. Given that ribosome assembly process primarily occurs in the nucleus, so we identified the nuclear PDCD2-associated proteins with mass spectrometry (MS). From the MS results, we identified that PDCD2 could interact with a family of RPS2 proteins including RPS2B (Supplementary Table 1). These interactions were further validated by yeast two-hybrid assay and split luciferase complementation (Fig. 2d, e). In our previous study, we proved the interaction between AtPRMT3 and RPS2 proteins[24], here, we also identified that PDCD2 could interact with AtPRMT3 validated by split luciferase complementation assay (Fig. 2f), co-immunoprecipitation (Supplementary Fig. 3b), and Bimolecular Fluorescence Complementation (BiFC) (Supplementary Fig. 3c).

To investigate whether *PDCD2-D1* could rescue the developmental defects of *rps2a2b-1* mutants, we crossed *pdcd2-d1* with *rps2a2b* to generate *rps2a2bpdcd2-d1* mutants. Remarkably, the *rps2a2bpdcd2-d1* mutants also exhibited a partial rescue of the developmental defects observed in *rps2a2b* mutants (Fig. 2g, h) as well as the pre-rRNA processing defects (Fig. 2i).

In summary, the collective biochemical and genetic evidences prove that PDCD2 has biological functions in regulating AtPRMT3-RPS2 mediated ribosome biogenesis process.

https://doi.org/10.1038/s41467-024-52945-8

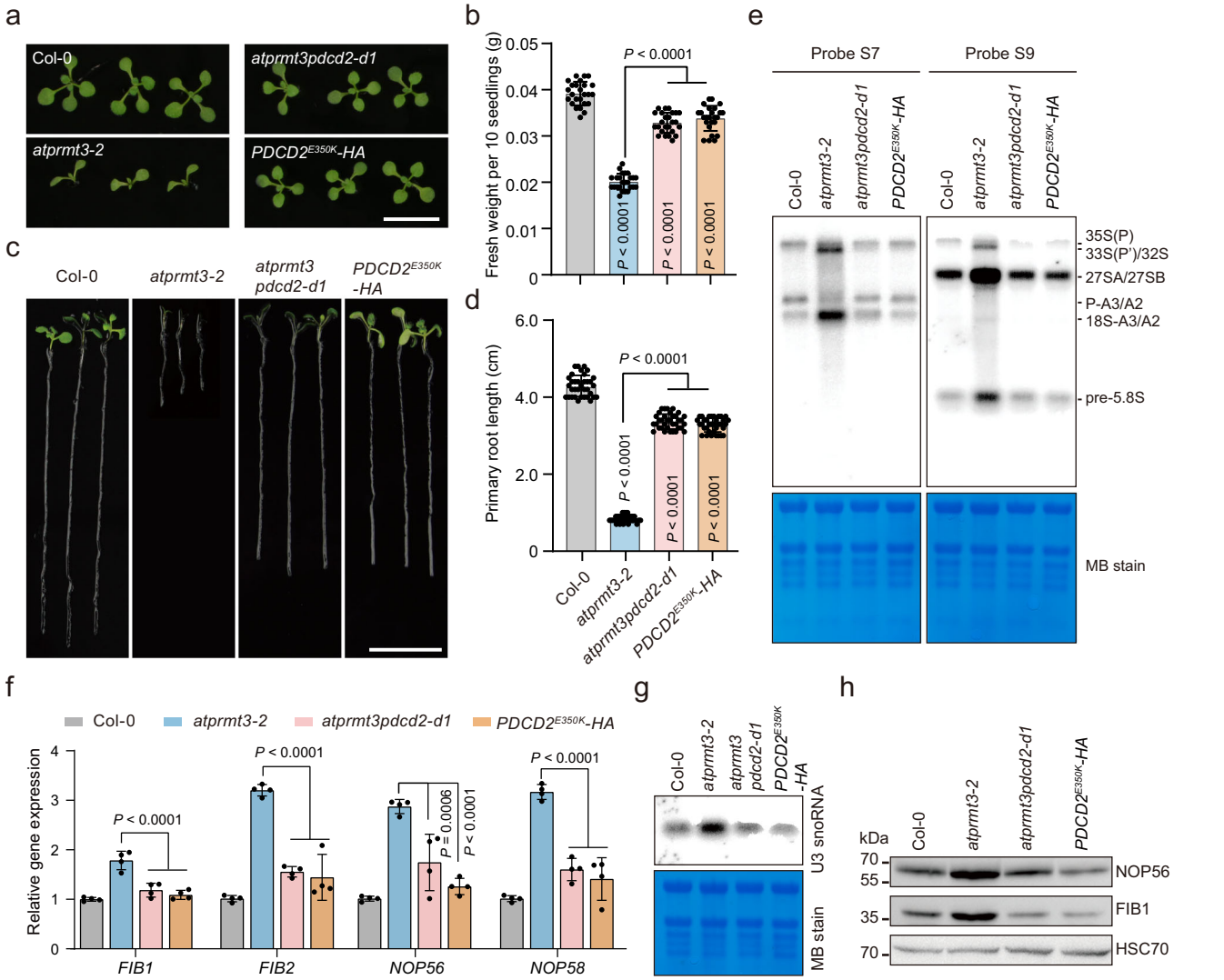

Fig. 1 | Mutation in *PDCD2* suppresses the defective development and ribosome biogenesis in *atprmt3* mutants. a, **b** Phenotypes of the aboveground seedlings. Ten-day-old seedlings of Col-0, *atprmt3-2*, *atprmt3pdcd2-d1*, and *PDCD2*^{E350K}*-HA* are shown. Scale bar, 1 cm. Data are presented as mean values ± SD (n = 25). **c**, **d** Phenotypes of primary root length. Nine-day-old seedlings were shown. Scale bar, 1 cm. Data are presented as mean values ± SD ($n = 35$). **e** Pre-rRNA processing states. Northern blot was performed with probe S7 and S9, methylene blue (MB) stain was used as a loading control. Experiments were repeated three times with similar results. **f** Gene expression patterns of *FIB1*, *FIB2*, *NOP56*, and *NOP58*, detected by qRT-PCR. *UBQ10* was used as an internal control. Data are presented as mean values ± SD ($n = 4$). **g** The expression of U3 snoRNA detected by Northern blot. Probe for U3 snoRNA was used, MB stain was used as a loading control. Experiments were repeated three times with similar results. **h** The protein levels of FIB1 and NOP56 detected by immunoblotting. Total proteins were immunoblotted with anti-FIB1, anti-NOP56, and anti-HSC70 antibodies. HSC70 was used as the control. Experiments were repeated two times with similar results. *P* value was calculated by One-way ANOVA with Dunnett's multiple comparisons test. Source data are provided as a Source Data file.

Mutation in *PDCD2* rescues the retarded pre-ribosome assembly in *atprmt3* mutants

The PDCD2-associated proteins also include U3 snoRNP proteins such as FIB1 and NOP56 (Supplementary Table 1). These interactions were further validated by co-immunoprecipitation (Supplementary Fig. 3d). We also observed that their associations were enhanced in *atprmt3-2* mutants, but partially reduced in suppressor *atprmt3pdcd2-d1* (Supplementary Fig. 3d). The above results indicate the potential function of PDCD2 in pre-ribosome biogenesis process.

We observed that the protein level of PDCD2 was accumulated in the nucleus, but decreased in cytoplasm in *atprmt3-2* mutants; the aberrant distribution was restored in the suppressor (Fig. 3a), indicating its potential disruptive transport between the cytoplasm and nucleus. Moreover, we used gel-filtration assay to show that more PDCD2 proteins were distributed in the high-molecular-weight fractions in *atprmt3-2* mutants, and PDCD2^{E350K} were returned to a normal level in suppressor (Fig. 3b). The above results suggest that PDCD2 is involved in the regulation of dynamic pre-ribosome biogenesis in the nucleus. Furthermore, we determined the distribution pattern of PDCD2 in cytoplasmic and the nuclear fractions, respectively. It was evident that nuclear PDCD2 was primarily distributed in the high-molecular-weight fractions; in contrast, cytoplasmic PDCD2 was mainly distributed in the low-molecular-weight fractions (Supplementary Fig. 3e). This observation further proves that PDCD2 functions in a large complex (including pre-ribosomes) in nucleus.

PDCD2 functions in nucleocytoplasmic transport

Interestingly, a series of proteins related to nucleocytoplasmic transport were also identified in PDCD2-associated proteins (Supplementary Table 1). The nuclear pore complex (NPC) comprises multiple copies of different nucleoporins (Nups), which forms a channel-like

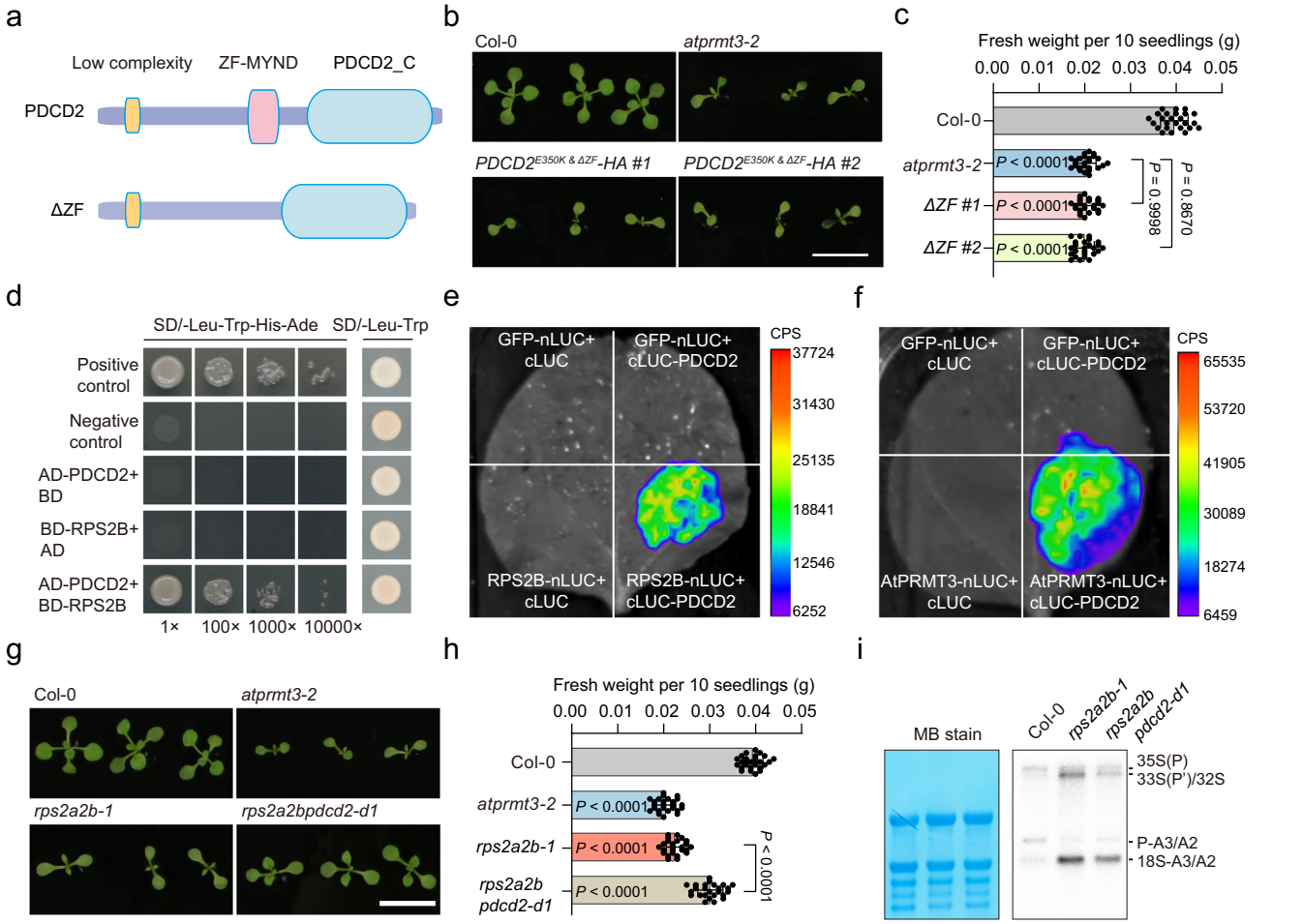

Fig. 2 | PDCD2 interacts with AtPRMT3 and RPS2B, and mutation of *PDCD2* partially rescues the defects of *rps2a2b* mutants. a Protein schematic structures of PDCD2 and its ΔZF version. **b**, **c** Phenotypes of ten-day-old seedlings of Col-0, *atprmt3-2*, and *PDCD2$^{E350K\&\Delta ZF}$-HA* are shown. Scale bar, 1 cm. Data are presented as mean values ± SD (n = 25). **d**, **e** The interaction between PDCD2 and RPS2B validated by yeast two-hybrid assay (**d**) and luciferase complementation assay (**e**). **f** The interaction between PDCD2 and AtPRMT3 validated by luciferase complementation assay. **g**, **h** Phenotypes of ten-day-old seedlings of Col-0, *rps2a2b-1*, and *rps2a2bpdcd2-d1* are shown. Scale bars, 1 cm. Data are presented as mean values ± SD (n = 25). **i** Pre-rRNA processing states. Northern blot was performed with probe S7, methylene blue (MB) stain was used as a loading control. All experiments were repeated at least three times with similar results. *P* value was calculated by One-way ANOVA with Dunnett's multiple comparisons test. Source data are provided as a Source Data file.

structure[11,26]. NPC controls macromolecular trafficking between the nucleus and the cytoplasm, including the transportation of pre-60S and pre-40S subunits[27]. Exportin 1 (XPO1), also known as chromosomal maintenance 1 (CRM1), is a major transport receptor, responsible for exporting proteins and multiple RNA species[28,29]. Then we wondered whether PDCD2 could transport though NPC in a XPO1-dependent manner. To address this, we analysed the localization of PDCD2-GFP following treatment with leptomycin B (LMB) which is a XPO1 inhibitor[30]. The results show that PDCD2-GFP is accumulated in the nucleus after LMB treatment, indicating that PDCD2 shuttles between the nucleus and the cytoplasm (Fig. 3c). In *Arabidopsis*, *XPO1* comprises two closely related members, *XPO1A* and *XPO1B*, with their single mutants exhibiting normal behavior, however, their double mutants display gametophytic defects[31], so it restricts us to perform downstream genetic experiment. Thus, we focused our attention on other NPC complex members for genetic validation, such as HOS1 (high expression of osmotically responsive genes 1). HOS1 was reported to interact with RNA export factor 1 (RAE1), Nup43, Nup96, and Nup160, and compromises a core region of plant NPCs[32–34]. We crossed *hos1-3* with the suppressor *atprmt3pdcd2-d1* to create *hos1atprmt3pdcd2-d1* triple mutants. The results showed that the *hos1atprmt3pdcd2-d1* triple mutants compromised the restoration capacity of the suppressor *atprmt3pdcd2-d1*, with the phenotypes of the *hos1atprmt3pdcd2-d1* triple mutants were between *atprmt3-2* and *atprmt3pdcd2-d1* suppressor (Fig. 3d, e). The results indicate that the suppressor *atprmt3pdcd2-d1* functions partially through the NPC function.

Furthermore, we performed data-independent acquisition (DIA) mass spectrometry (MS) to determine the difference of nuclear proteins in Col-0, *atprmt3-2*, and *atprmt3pdcd2-d1* (Fig. 3f). We found that most of the accumulated proteins in *atprmt3-2* mutants were restored in suppressor *atprmt3pdcd2-d1* (Fig. 3f), those restored proteins were mainly associated with ribonucleoprotein complex biogenesis and ribosome biogenesis (Fig. 3g, Supplementary Data 1). Additionally, we performed RNA fluorescence in situ hybridization (RNA-FISH) to detect the pre-rRNA expression pattern. We visualized that the pre-rRNA signals were retarded in *atprmt3-2* mutants with a large nucleolus, but restored in suppressor *atprmt3pdcd2-d1* (Fig. 3h). As a result, our findings provide compelling evidence that PDCD2 plays a role in the export of pre-ribosomes to the cytoplasm. Notably, the PDCD2^{E350K} facilitate the translocation of delayed pre-ribosomes to the cytoplasm in *atprmt3-2* mutants, thereby partially rescuing their aberrant ribosome biogenesis.

Finally, we investigated the ribosome state in the suppressors, finding that *atprmt3pdcd2-d1* also rescued the aberrant polysome state in *atprmt3-2* mutants (Fig. 4a, b). Additionally, genome-wide gene

https://doi.org/10.1038/s41467-024-52945-8

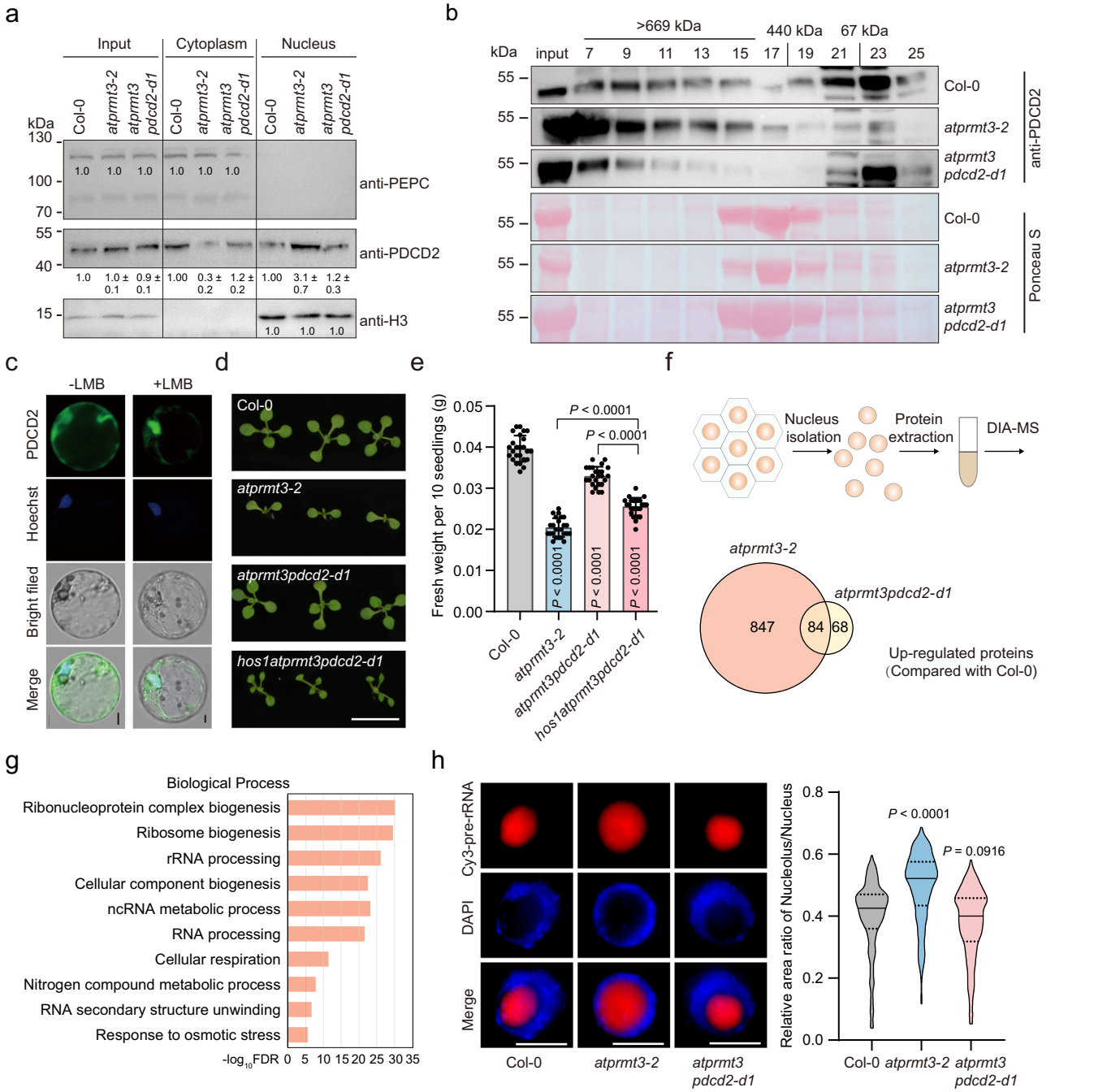

Fig. 3 | The retarded pre-ribosome assembly in *atprmt3* mutants is rescued by mutation of *PDCD2*. **a** The subcellular distribution of PDCD2/PDCD2^{E350K} from Col-0, *atprmt3-2*, and *atprmt3pdcd2-d1*. Protein lysates were immunoblotted with anti-PDCD2, anti-PEPC, and anti-H3 antibodies after subcellular fractionation. PEPC (phosphoenolpyruvate carboxylase) and histone H3 were used as markers for cytoplasm and nucleus, respectively. Data are presented as mean values ± SD ($n = 3$). **b** Gel filtration patterns of PDCD2/PDCD2^{E350K} in Col-0, *atprmt3-2*, and *atprmt3pdcd2-d1*. Protein lysates were fractioned by gel filtration and immunoblotted with anti-PDCD2 antibody. Ponceau S staining was used as a control. Experiments were repeated two times with similar results. **c** Protoplast expressing PDCD2-GFP treated with or without leptomycin B (LMB) ($n = 20$). Nucleus are stained by Hochest in blue. Scale bar, 5 μm. Experiments were repeated two times with similar results. **d**, **e** Phenotypes of Col-0, *atprmt3-2*, *atprmt3pdcd2-d1*, and *hos1atprmt3pdcd2-d1*. Scale bar, 1 cm. Data are presented as mean values ± SD ($n = 25$). **f** Schematic of the DIA-MS analysis. Nuclear protein from Col-0, *atprmt3-2*, and *atprmt3pdcd2-d1* were applied for MS ($n = 3$). Venn diagram showed the up-regulated proteins in *atprmt3-2*, and *atprmt3pdcd2-d1* compared with Col-0. $P < 0.0001$ was calculated by two-sided Fisher's exact test. **g** Gene Ontology analysis (Biological Process) of the 847 proteins in (**f**). **h** The RNA FISH of pre-rRNAs in Col-0, *atprmt3-2*, and *atprmt3pdcd2-d1*. Pre-rRNAs are probed by Cy3-S7, DAPI stain is the nucleus, scale bar, 5 μm. Violin plot shows the quantitative measurement of nucleolar area ratio (nucleolus/nucleus) ($n = 248, 226, 234$). The horizontal solid lines represent the median; the horizontal dashed lines represent the quartile. Experiments were repeated two times with similar results. *P* value was calculated by One-way ANOVA with Dunnett's multiple comparisons test. Source data are provided as a Source Data file.

https://doi.org/10.1038/s41467-024-52945-8

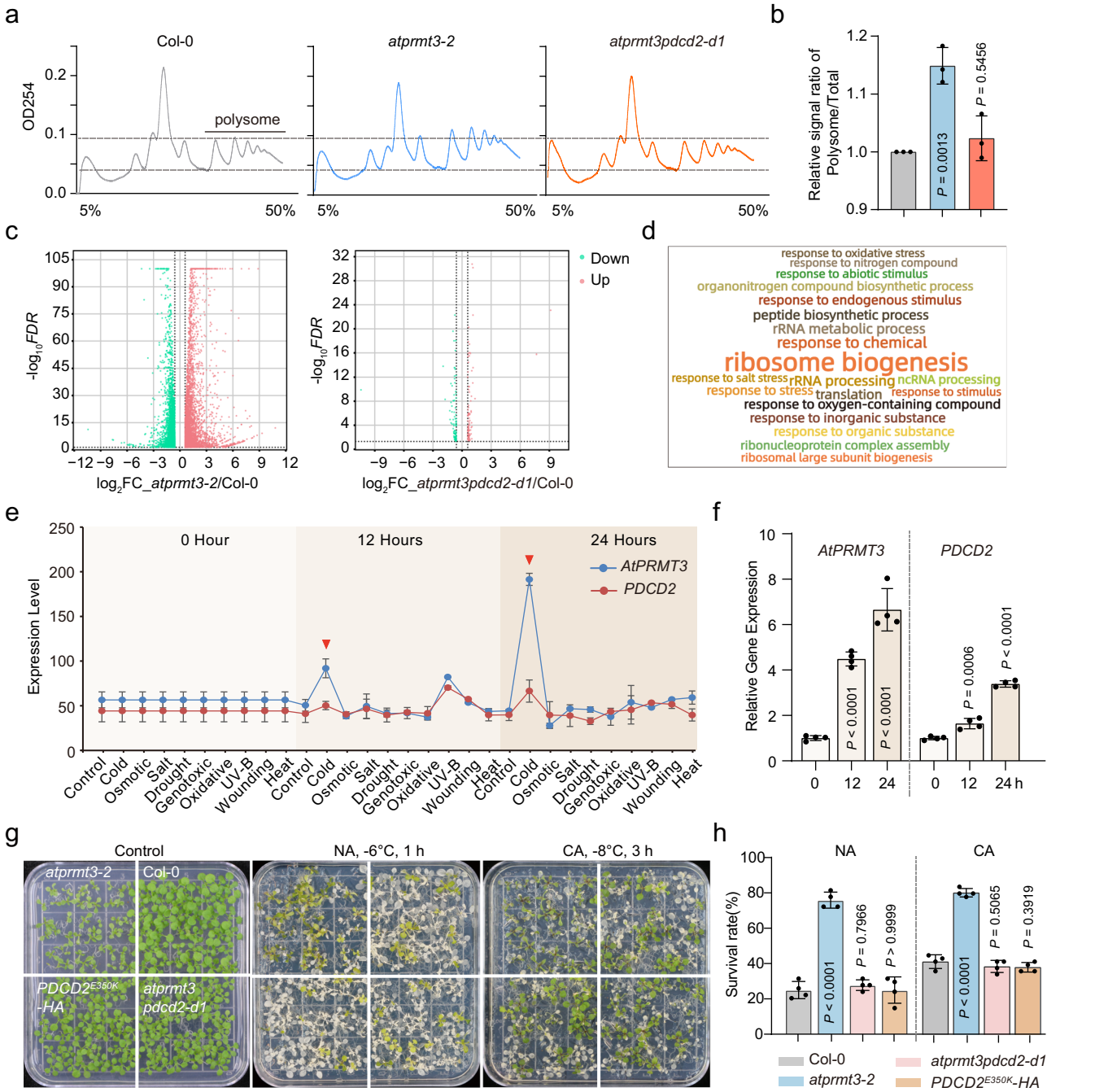

Fig. 4 | The *atprmt3* mutants exhibit freezing tolerant phenotype and rescued by mutation of *PDCD2*. **a** Polysome profiles of Col-0, *atprmt3-2*, and *atprmt3pdcd2-d1*. The *x*-axis indicates 5–50% sucrose gradient, *y*-axis indicates OD254. **b** Statistical analysis for relative OD254 signal ratios of polysome/total in (**a**). Data are presented as mean values ± SD (n = 3). **c** Volcano plots of differentially expressed genes in *atprmt3-2* and *atprmt3pdcd2-d1* compared with Col-0. **d** Gene ontology (Biological process) of the up-regulated genes that are rescued in suppressor *atprmt3pdcd2-d1*. Font size correlates to -Log_{10}FDR. **e** The expression pattern of *AtPRMT3* and *PDCD2* in shoot under various abiotic stress conditions. Data are presented as mean values ± SD. **f** The expression of *AtPRMT3* and *PDCD2* in response to cold stress. Total RNA from twelve-day-old Col-0 seedlings treated at 4 °C for 0, 12, and 24 h were used for qRT-PCR. *UBQ10* was used as internal control. Data are presented as mean values ± SD (n = 4). **g** Freezing stress phenotypes. Twelve-day-old seedlings of Col-0, *atprmt3-2*, *atprmt3pdcd2-d1*, and complementation lines *PDCD2*^{E350K}*-HA* were subjected to freezing treatment at −6 °C for 1 h for non-acclimated (NA) condition or −8 °C for 3 h for cold-acclimated (CA) condition. **h** The survival rates of plants in (**g**). Data are presented as mean values ± SD (n = 4). *P* value was calculated by One-way ANOVA with Dunnett's multiple comparisons test. Source data are provided as a Source Data file.

expression analysis revealed that the suppressor restored most of the differentially expressed genes in *atprmt3-2* mutants (Fig. 4c, Supplementary Data 2). Gene ontology analysis of these rescued up-regulated genes showed that they were mainly associated with ribosome biogenesis, highlighting the role of AtPRMT3-PDCD2 in ribosomal functions (Fig. 4d). Moreover, we observed the enrichment of stress-responsive genes in this process (Fig. 4d), implying the involvement of AtPRMT3-PDCD2 in stress response.

AtPRMT3-PDCD2 functions in freezing stress response

Then we are curious about whether AtPRMT3 or PDCD2 is involved in stress responses. Firstly, we detected the expression of *AtPRMT3* and

PDCD2 in response to multiple stresses from public database, and found that they were obviously induced by cold stress (Fig. 4e)[35]. Further validation through qRT-PCR confirmed the upregulation of *AtPRMT3* and *PDCD2* upon cold treatment (Fig. 4f). This led us to investigate the potential involvement of *AtPRMT3* in freezing stress adaptation. To do so, we subjected twelve-day-old seedlings grown at 22 °C to freezing treatment with cold acclimation (CA) or non-acclimation (NA). The results showed that under both NA and CA conditions, *atprmt3-2* mutants displayed enhanced freezing tolerance compared with wild-type Col-0 (Fig. 4g, h). These results suggest that AtPRMT3 is a negative regulator in freezing tolerance. Furthermore, the suppressor *atprmt3pdcd2-d1* was able to rescue the freezing tolerant phenotype of *atprmt3-2* mutants under both NA and CA conditions (Fig. 4g, h).

AtPRMT3 regulates freezing stress mainly through CBF-independent pathways

The CBF/DREB 1 (C-Repeat Binding Factor/Dehydration Responsive Element Binding protein 1)-dependent pathway plays a vital role in cold stress regulation[4]. Therefore, we detected whether AtPRMT3 mediates plants responses to cold stress through the CBF pathway. We compared the expression levels of *CBF1/2/3*, and their targets including *RD29A*, *COR15B*, and *KIN1* in Col-0 and *atprmt3-2* mutants under cold stress. These results showed that the expression of *CBFs* and their targets did not exhibit consistent up-regulation pattern in *atprmt3-2* mutants (Supplementary Fig. 4a, b), suggesting that AtPRMT3 was involved in freezing stress partially through CBF pathway. Moreover, we crossed *atprmt3-2* with *cbfs* (*cbf1cbf2cbf3*) triple mutants to create *atprmt3cbfs* quadruple mutants to identify their freezing tolerance. Under both CA and NA conditions, *atprmt3cbfs* mutants demonstrated increased tolerance to freezing stress compared with Col-0 (Supplementary Fig. 4c, d). Under CA conditions *atprmt3cbfs* mutants also show reduced survival rate compare to *atprmt3-2* mutants, suggesting the partial function of CBFs in this process (Supplementary Fig. 4c, d). The freezing tolerant phenotype of *atprmt3* mutants in NA conditions indicating their stronger response to cold stress, and our work focuses on understanding the mechanism through which they are regulated under these conditions.

AtPRMT3-RPS2 modulates transcriptome and translatome homeostasis

RPS2 is the direct component of ribosome, and RPS2 family has four members including RPS2A, RPS2B, RPS2C, and RPS2D. For our study, we focused on the phenotypically distinct pair of mutants *rps2a2b-1* and *rps2c-1* to assess their response to freezing stress. We found that *rps2a2b-1* mutants were tolerant to freezing stress like *atprmt3-2* mutants, whereas *rps2c-1* mutants were sensitive to freezing like Col-0 (Fig. 5a, b). These results indicate that although the members of RPS2 are core component of ribosome, but they possess different functions, which may imply their heterogeneous nature within ribosome function.

Next, we detected the translation state in Col-0, *atprmt3-2* and *rps2* mutants with polysome profiling. Remarkably, we observed a significant increase in the polysome ratios in both *atprmt3-2* and *rps2a2b-1* mutants, while the polysome pattern of the *rps2c-1* mutant remained comparable to that of Col-0 (Fig. 5c, d). These results imply that AtPRMT3 and RPS2A2B are involved in the regulation of translation dynamics, and then it inspires us to examine their effect on mRNA translation. Ribo-seq analysis enables genome-wide investigation of translation[36–38]. To get a comprehensive view of the translational regulation, we performed RNA-seq and Ribo-seq to assess their transcriptional and translational changes, respectively (Fig. 5e). The independent Ribo-seq and RNA-seq library replicates showed high reproducibility (Supplementary Fig. 5).

We computed the fold change (FC) of *atprmt3-2*, *rps2a2b-1*, and *rps2c-1* mutants compared with Col-0 for transcriptome (RNA-seq), translatome (Ribo-seq) and translational efficiency (TE, TE=Ribo-seq_RPKM/RNA-seq_FPKM). We compared the changes between transcriptome and translatome, and observed a moderate correlation ($R \approx 0.4$) between translational (Ribo-seq) and transcriptional changes (RNA-seq) in *atprmt3* and *rps2a2b* mutants (Fig. 5f), which suggests the presence of a regulatory mechanism at the translational level in these mutants. Additionally, the results provided evidence of similar translation states between *atprmt3-2* and *rps2a2b-1* mutants, in contrast to *rps2c-1* mutants (Fig. 5f). To better illustrate the translational changes, we calculated the translational efficiency (TE) to quantify these changes and found that alternations in TE have poor correlations with the transcription changes (Supplementary Fig. 6), which further indicates that extra layer of translational regulation.

Given the similar phenotypes exhibited in *atprmt3-2* and *rps2a2b-1* mutants, we compared genes that were altered in both mutants, excluding *rps2c-1* mutants. We identified 724 genes with down-regulated TE, mainly associated with growth-related genes such as Carbohydrate metabolic process, Cell wall organization or biogenesis, and Reproductive system development (Fig. 6a, c, and Supplementary Data 3). Interestingly, the 648 genes with up-regulated TE were primarily associated with stress responses such as Response to stimulus, Response to reactive oxygen species, and Response to cold (Fig. 6b, d, and Supplementary Data 3).

Altogether, the above results suggest that AtPRMT3-RPS2 is a vital regulator in translational regulation process, maintaining a delicate balance between the translation of stress-responsive and growth-related processes.

The disruption of AtPRMT3-RPS2B promotes the expression of stress responsive genes

Next, we compared these 648 specifically TE up-regulated genes with cold-induced genes, finding that nearly 20% of these genes are cold inducible, potentially contributing to the freezing-tolerant phenotype of *atprmt3-2* mutants (Supplementary Fig. 7a, and Supplementary Data 4). We observed that the expression of *Chaltone synthase* (*CHS*) was accumulated in *atprmt3-2* and *rps2a2b-1* mutants instead of *rps2c-1* (Fig. 6e), which was further validated by qRT-PCR (Fig. 6f). The translation efficiency of *CHS* was also accumulated in *atprmt3-2* and *rps2a2b-1* mutants instead of *rps2c-1* (Fig. 6g), corresponding to the higher protein level of CHS in *atprmt3-2* and *rps2a2b-1* mutants (Supplementary Fig. 7b). And the expression of *CHS* was induced by cold stress (Fig. 6h). CHS serves as a key enzyme in the flavonoid biosynthesis pathway (Supplementary Fig. 7c). Flavonoid is a major class of secondary plant metabolites and is essential for plant development and plant–environment interplay[39]. Then we detected gene expression of key enzymes in flavonoid metabolic pathway, finding that most of these genes including *CHI*, *DFR*, *ANS*, and *FLS1* all exhibited an up-regulated gene expression pattern in *atprmt3-2* and *rps2a2b-1* mutants instead of *rps2c-1* mutants (Supplementary Fig. 7d, e). We found that the TE of *FLS1* and *ANS* was also accumulated in *atprmt3-2* and *rps2a2b-1* mutants instead of *rps2c-1* (Supplementary Fig. 7f). The flavonoid including anthocyanin facilitates plants adaptation to cold stress[40,41]. We identified that there were higher levels of anthocyanin in *atprmt3-2* and *rps2a2b-1* mutants compared with Col-0 and *rps2c-1* mutants (Supplementary Fig. 7g). Furthermore, we generated a *chs* mutant with CRISPR-Cas9 (Supplementary Fig. 7h) and crossed it with *atprmt3-2* to create *atprmt3chs* double mutants, finding that the freezing tolerance ability of *atprmt3chs* double mutants was reduced compared with *atprmt3-2* mutants (Fig. 6i, j), which partially explains its freezing tolerant phenotype.

Collectively, we revealed that AtPRMT3-RPS2 function as a translational regulator to balance the translation of genes involved in

https://doi.org/10.1038/s41467-024-52945-8

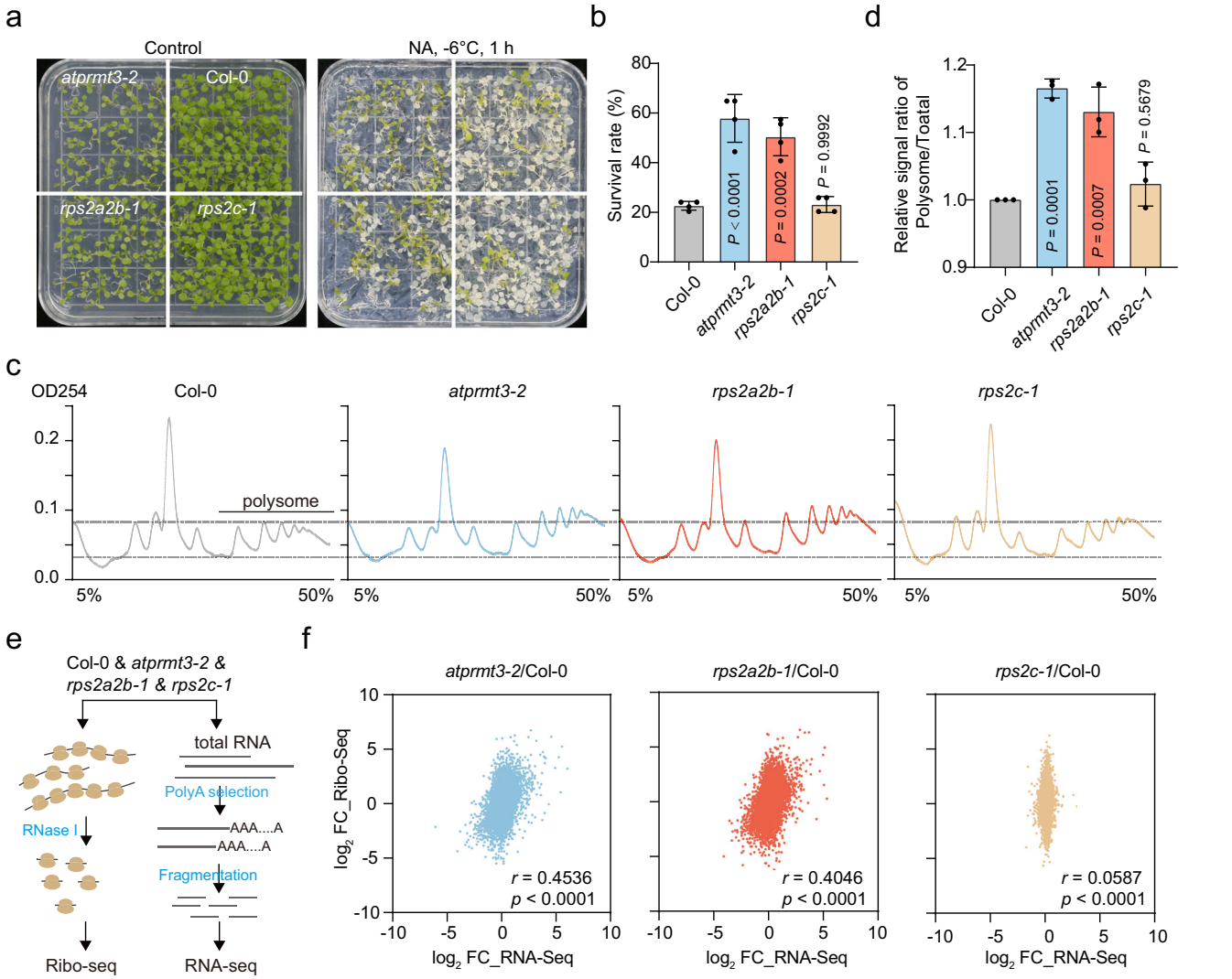

Fig. 5 | AtPRMT3-RPS2 co-regulate transcriptome and translatome changes. **a** Freezing stress phenotype. Twelve-day-old seedlings of Col-0, *atprmt3-2*, *rps2a2b-1*, and *rps2c-1* were subjected to freezing treatment at −6 °C for 1 h under NA condition. **b** The survival rates of plants in (**a**). Data are presented as mean values ± SD (n = 4). **c** Polysome profiles of Col-0, *atprmt3-2*, *rps2a2b-1*, and *rps2c-1* mutants. The *x*-axis indicates 5–50% sucrose gradient, *y*-axis indicates OD254. **d** Statistical analysis for relative OD254 signal ratios of polysome/total in (**c**). Data are presented as mean values ± SD (n = 3). **e** Schematic representation of RNA-seq and Ribo-seq analysis. **f** The correlation between translational and transcriptional changes. Scatter plots comparing fold-changes (FC) of FPKM between RNA-seq (*x*-axis) and Ribo-seq (*y*-axis) are shown. Pearson *r* and two-tailed *p* value are shown. (**b, d**) *P* value was calculated by One-way ANOVA with Dunnett's multiple comparisons test. Source data are provided as a Source Data file.

growth and stress responses (Supplementary Fig. 8). In wild type, AtPRMT3-RPS2B promotes the proper pre-ribosome assembly in nucleus, and PDCD2 promotes efficient pre-ribosome export to cytoplasm, ultimately maintaining normal translation in the cytoplasm and promoting the expression of genes related to growth. However, the defects of AtPRMT3-RPS2B results in disturbed ribosome biogenesis and translation, whereby promoting the expression of stress responsive genes (such as cold related genes), therefore conferring freezing tolerant phenotypes (Supplementary Fig. 8).

Discussion

Translation is a fundamental process required for all cellular activities. Impairments in ribosome or translation are associated with multiple developmental defects and stress responsive disorders. Previously, we show that AtPRMT3-RPS2B actively promotes pre-ribosome assembly and alleviates nucleolus stress[24]. Here, we further demonstrated the molecular mechanism of AtPRMT3-RPS2B in ribosome assembly process, and its pivotal role in orchestrating the balance between the translation of genes associated with growth and stress response.

The membrane-less nucleolus serves as the primary site for ribosome biogenesis, and alterations in ribosome biogenesis often manifest in changes to nucleolar organization[42,43]. We found that *atprmt3* mutants exhibit enlarged nucleolus due to retarded pre-ribosome assembly in nucleus. Here, we identified that *PDCD2-D1* rescued the aberrant ribosome biogenesis and nucleolar stress in *atprmt3* mutants. PDCD2 is conserved in different species, its homolog PDCD2/PDCD2L in human and TSR4 in yeast, were reported to cooperate with RPS2/uS5, which function in ribosome biogenesis[44–46]. Here, we proved that *Arabidopsis* PDCD2 was required for dynamic pre-ribosome assembly by exporting the ribosome subunit to cytoplasm in time. The NPC is the trafficking gateway for macromolecular cargos between the nucleus and the cytoplasm, pre-ribosomal particles are among the largest transport cargos[8]. PDCD2 shuttles between nucleus and cytoplasm. PDCD2-D1 promotes the export of pre-ribosome subunits in *atprmt3-2* mutants, thereby relieving their retarded pre-ribosome assembly in nucleus.

In plants, nuclear pore complexes are recognized for their pivotal roles in response to both biotic and abiotic stresses, including

https://doi.org/10.1038/s41467-024-52945-8

immunity and temperature responses[10,12]. For example, HOS1 and LOS4 emerging as key players associated with NPC in cold stress[47,48]. Our study reveals a novel dimension related to NPCs in regulating cold stress. Specifically, we elucidate that AtPRMT3-RPS2-PDCD2 primarily functions to facilitate ribosome biogenesis from the nucleus to the cytoplasm through NPC, thereby ensuring the accurate translation step in the cytoplasm. During cold stress, the expression of *CBFs-CORs* is an essential step, but only 10-20% of *CORs* are transcriptionally

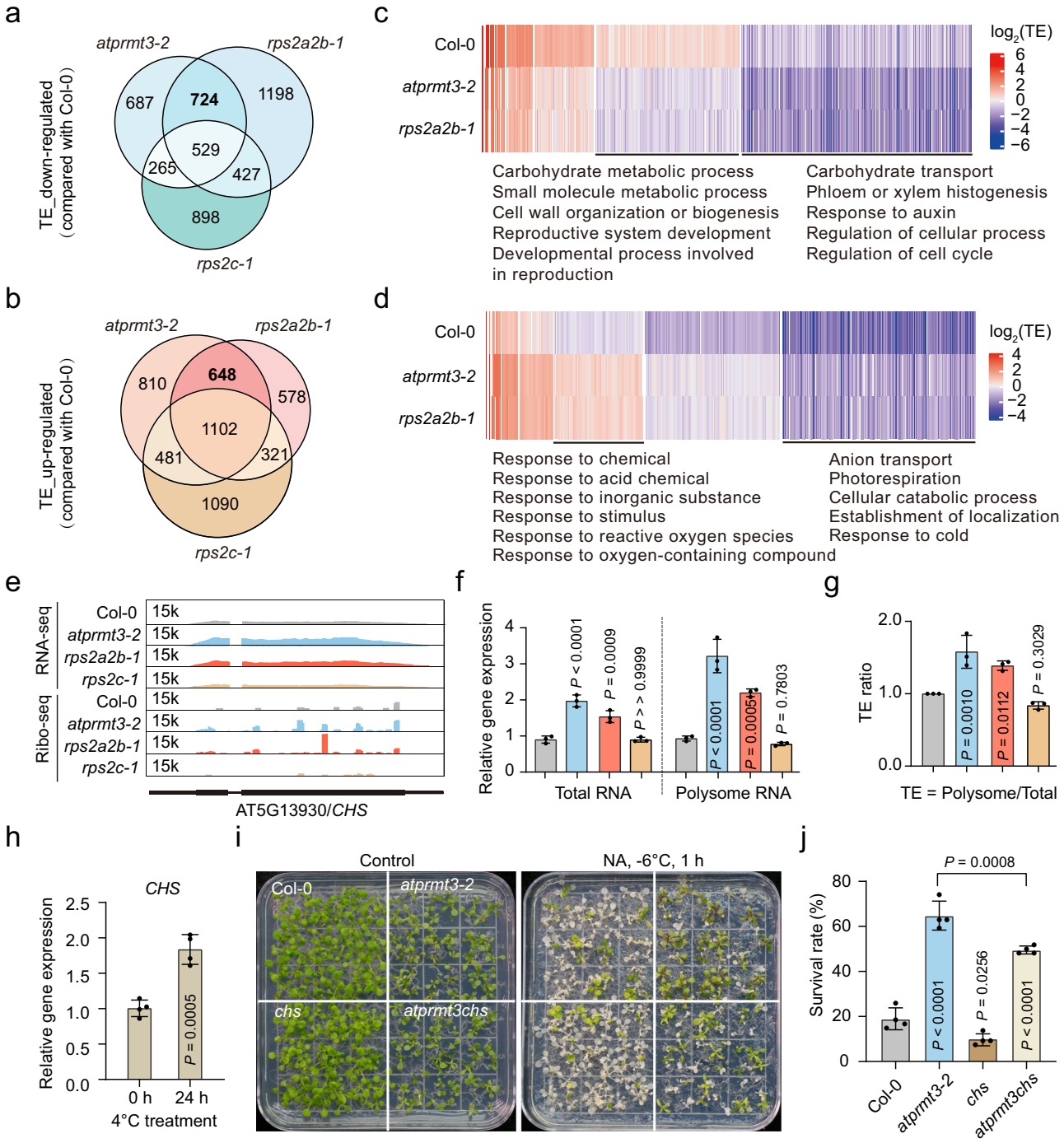

Fig. 6 | AtPRMT3-RPS2 balances the trade-off between a general growth and stress-responsive state. a, **b** Venn diagrams illustrating down-regulated (**a**) and up-regulated (**b**) Translational Efficiency (TE). **c**, **d** The heatmaps showing up-regulated and down-regulated TE. Heatmap (**c**) was genes with down-regulated TE in *atprmt3-2* and *rps2a2b-1* excluding *rps2c-1* (724 in **a**). Heatmap (**d**) was genes with up-regulated TE in *atprmt3-2* and *rps2a2b-1* excluding *rps2c-1* (648 in **b**). The heatmap encompasses eight groups based on the patterns of their translational status, with representative enriched Gene Ontology (GO) terms shown. The $\log_2$(TE) is shown by the color scale. **e** Representative genome browser view of RNA-seq and Ribo-seq for *CHS*. **f** Expression validation for *CHS*. Total RNA and polysome RNA from Col-0, *atprmt3-2*, *rps2a2b-1*, and *rps2c-1* mutants were used for qRT-PCR. *ACTIN2* was used as a control. Data are presented as mean values ± SD (n = 3). **g** Translation efficiency analysis in (**f**). Data are presented as mean values ± SD (n = 3). **h** Induction of *CHS* expression by cold stress. Twelve-day-old seedlings of Col-0 were treated at 4 °C for 0 and 24 h, and then used for qRT-PCR. *ACTIN2* was used as a control. Data are presented as mean values ± SD (n = 4). **i** Freezing stress phenotype. Twelve-day-old seedlings of Col-0, *atprmt3-2*, *chs* and *atprmt3chs* were subjected to freezing treatment at −6 °C for 1 h for non-acclimated (NA) condition. **j** The survival rates of plants in (**i**). Data are presented as mean values ± SD (n = 4). (**f**, **g**, **j**) *P* value was calculated by One-way ANOVA with Dunnett's multiple comparisons test. (**h**) *P* value was calculated by two-sided unpaired Student's *t* test. Source data are provided as a Source Data file.

regulated by *CBFs*[4,49,50]. It is interesting to investigate CBF-independent regulating mechanisms, such as the Nonexpresser of pathogenesis-related genes 1 (NPR1) and Brassinazole-resistant 1 (BZR1)[51,52]. The ribosome recognized as cold stress sensors, is known to be affected by cold stress, influencing both rRNA biogenesis and gene expression related to ribosomes[53–55]. Accumulating evidence highlights the essential role of ribosomes in cold stress adaptation, with factors such as Ribosomal Protein L9 (RPL9) and cytosolic ribosomal biogenesis factor REI-LIKE (REIL) implicated in this process[56–58]. Our findings contribute to this understanding by revealing a translational mechanism involving AtPRMT3-RPS2B. This complex acts as a translation regulator balancing trade-off of growth and stress-responsive gene expression. Defects in AtPRMT3 promote the translation of cold stress-responsive gene expression, endowing the *atprmt3* mutants with a freezing-tolerant phenotype.

Ribosome is dynamic and not uniform in its structural composition. Our study demonstrates that *rps2* family mutants exhibit diverse phenotypes and translation status, it will be interesting to study whether it is due to ribosome heterogeneity in the future. Ribosome heterogeneity includes sequence variation of rRNAs, absence of specific ribosomal proteins (RP), modification of rRNAs/RPs, different auxiliary factors, etc[59,60]. Evidence shows that heterogeneous ribosomes preferentially translate different subpools of mRNAs[61]. The intrinsic features existed in mRNA also determine the efficiency of translation, such as UTR, polyA tail, as well as secondary structures within mRNA[13,62]. Particularly upstream open reading frames (uORFs) is small ORFs located in the 5′ UTR, which repress the translation of the downstream ORF[63]. It remains to determine whether the mRNA features affect translation in these ribosome-defective mutants. Ribosome is the translation machine in cells, the response of ribosome biogenesis to stress adds fine-tuning layer to the regulation of gene expression. Translational regulation provides valuable insights for crop breeding with improved stress tolerance and high quality[64]. Therefore, the understanding of ribosome feature and translational mechanism is particularly noteworthy, which can be used for modern agricultural breeding in the future.

Methods

Plant materials

The materials used in this study including *atprmt3-2* (WISCDSLOX391A01), *rps2c-1* (SALK_020959C) and *rps2a2b-1* mutants were characterized previously[23,24]. The *chs* mutants were created by CRISPR-Cas9[65].

EMS mutagenesis and DNA sequencing

The seeds of *atprmt3-2* mutants were mutagenized with ethyl methanesulfonate (EMS). The resulting individual M1 plants were screened to isolate suppressors of *atprmt3-2* mutants. The identified suppressors were backcrossed with *atprmt3-2* for at least three times. Homogenous seedlings exhibiting wild-type characteristics were selected for DNA extraction and underwent whole-genome resequencing at Berry Genomics. Simultaneous Identification of Multiple causal Mutations (SIMM) analysis was employed to clone the suppressor genes[66].

Plasmid construction and generation of transgenic plants

The CDS of $PDCD2^{E350K}$ amplified from *m20* cDNA was cloned to generate the *ProUBQ10:*$PDCD2^{E350K}$*-HA* constructs, and then transformed into *atprmt3-2* mutants to generate $PDCD2^{E350K}$*-HA* plants. The constructs *ProUBQ10:*$PDCD2^{E350K\&\Delta ZF}$*-HA* was generated on basis of *ProUBQ10:*$PDCD2^{E350K}$*-HA*, and transformed into *atprmt3-2* mutants to generate $PDCD2^{E350K\&\Delta ZF}$*-HA* plants. The CDS region of *PDCD2* amplified from Col-0 cDNA was cloned to generate the *ProUBQ10:PDCD2-GFP* constructs, and then transformed into Col-0 to generate *PDCD2-GFP*/Col-0 plants. The primers used in this study are listed in Supplementary Table 2.

Freezing treatment assay

Twelve-day-old seedlings grown at 22 °C were treated with or without cold acclimation (4 °C for 3 days), and then placed in freezing chamber initially set at 0°C and gradually decreased by 1°C per hour until the desired temperature. After freezing treatment, the plants were kept at 4 °C in dark overnight and then transferred to 22 °C for two or three days. Finally, the survival rates of the seedlings were counted. The germination rates of *atprmt3chs* double mutants are affected, in order to better calculate the survival rate, we replaced the ungerminated seeds before freezing assay.

Polysome profile

Polysome profile was performed as previously described[67]. Briefly, polysomes were extracted from 5 g twelve-day-old seedlings lysed with extraction buffer (0.2 M Tris-HCl, pH 9.0, 0.025 M EGTA, 0.2 M KCl, 0.035 M $MgCl_2$, 1% Brij-35, 1% CA630, 1% Triton X-100, 1% Tween-20, 1% sodium deoxycholate, 1% polyoxycholate 10 tridecyl ether, 1 mM PMSF, 5 mM DTT, 50 μg/mL cycloheximide, 50 μg/mL chloramphenicol and 0.5 mg/mL heparin). Then the supernatant was separated by sucrose cushion buffer (0.4 M Tris-HCl, pH 9.0, 0.2 M KCl, 0.005 M EGTA, 0.035 M $MgCl_2$ and 1.75 M sucrose), ultracentrifuged at 115,510 g (70Ti rotor) for 18 h at 4 °C. The polysome pellet was resuspended in resuspension buffer (0.2 M Tris-HCl, pH 9.0, 0.025 M EGTA, 0.2 M KCl, 0.035 M $MgCl_2$, 5 mM DTT, 50 μg/mL cycloheximide, 50 μg/mL chloramphenicol). A total of 3,500 OD260 units of the resuspension was separated by a linear 5–50% sucrose gradient, and ultracentrifuged at 213,669 g (SW-41Ti rotor) for 3 h at 4 °C. The samples were then analyzed by Piston Gradient Fractionator by monitoring OD254.

Northern blot

Briefly, 0.1 g twelve-day-old seedlings were used to extract total RNA with TRIzol reagent (TIANGEN, DP405). 5 μg total RNA was separated on a 1.2% agarose/formaldehyde gel and transferred to Hybond N^+ membrane (GE Healthcare). The γ-^{32}P-ATP labeled DNA probes were hybridized to the membrane. The membranes are exposed to a phosphor screen (GE Healthcare), and then the signals are detected by the Typhoon TRIO scanner (GE Healthcare).

Mass spectrometry (MS)

For the IP-MS analysis, the nuclear proteins from Col-0 were immunoprecipitated with anti-PDCD2 and anti-IgG antibodies, separated by SDS-PAGE gel (GenScript, M00664), and subjected to Coomassie blue staining. The proteins were then excised from the gel, subjected to in-gel digestion, and the resulting solution was analyzed with MS.

For Data-independent Acquisition (DIA) MS analysis, the nuclear protein from Col-0, *atprmt3-2*, and suppressor *m20* with three biological replicates were extracted, homogenized, and lysed in buffer containing 8 M urea, 0.1 M Tris-HCl (pH 8.0), protease inhibitor. The proteins were reduced with 10 mM DTT for 2 h, followed by alkylated with 20 mM iodoacetamide in the dark for 30 min. The protein solution was diluted 1:5 with 50 mM triethylammonium bicarbonate (TEAB) and digested with trypsin (1:50) at 37 °C overnight. The digestion was desalted on OASIS HLB column and peptides eluted with 60% acetonitrile were lyophilized via vacuum centrifugation.

The nanoLC-MS/MS experiments were performed on a Orbitrap Eclipse equipped with Easy n-LC 1200 HPLC system (Thermo Scientific). The MS analysis was performed with Orbitrap Eclipse mass spectrometer with the data-dependent acquisition mode (for IP-MS) or data-independent acquisition mode (for DIA-MS). The IP-MS data were analyzed with Proteome Discovery version 2.4.1.15 using Sequest HT search engine for protein identification. The DIA raw data were analyzed using Spectronaut version 18 (Biognosys) with the "DirectDIA" mode for protein identification and quantification. The Uniprot *Arabidopsis thaliana* protein database was used for searching the data.

Two missed cleavages were allowed for searching. FDR < 1% was set for both peptides and proteins identification. Proteins with $P < 0.05$ and fold change ≥ 1.5 were considered as differentially expressed.

Yeast-two-hybrid

The CDSs of *PDCD2* and *RPS2B* were cloned into pGADT7 and pGBKT7 (Clontech) to generate AD-PDCD2 and BD-RPS2B, respectively. Yeast-two-hybrid assay was performed according to the Matchmaker GAL4 Two-Hybrid System 3 (Clonetch). The constructs were transformed into the yeast strain AH109, which were grown on SD/-Leu-Trp. Then the transformants were selected on SD/-Leu-Trp-His-Ade. The primers used in this study are listed in Supplementary Table 2.

Luciferase complementation assay

The CDSs of *RPS2B* and *AtPRMT3* were cloned into the *pCAMBIA-split_nLUC* vector, generating *RPS2B-nLUC* and *AtPRMT3-nLUC*; The CDSs of *PDCD2* were cloned into the *pCAMBIA-split_cLUC* vector, generating *cLUC-PDCD2*[68]. Constructs were transformed into *Agrobacterium GV3101*, and co-infiltrated into *N. benthamiana* leaves. The luciferase activity was detected after two days with CCD imaging apparatus (CHEMIPROHT 1300B/LND; Roper Scientific). The primers used in this study are listed in Supplementary Table 2.

Bimolecular fluorescence complementation (BiFC)

The CDSs of *AtPRMT3* and *PDCD2* were cloned into the BiFC vector to generate *AtPRMT3-YFP-C* and *PDCD2-YFP-N*, respectively[69]. Constructs were transformed into *Agrobacterium GV3101*, and co-infiltrated into *N. benthamiana* leaves with different combinations. The leaves were analyzed by fluorescence microscope after two days. The primers used in this study are listed in Supplementary Table 2.

RNA fluorescence in situ hybridization (RNA-FISH)

RNA FISH was carried out according to the protocol previously described[70]. Briefly, 7-day-old seedlings were fixed in 4% methanol-free formaldehyde (Thermo Fisher Scientific, UK) for 30 mins and then washed three times with 1 × PBS before being squashed. Then the roots were left to dry for 1 h before being immersed in 70% ethanol for 1 h. Samples were then equilibrated with freshly prepared 10 % (v/v) deionized formamide (Thermo Fisher Scientific, UK) Stellaris RNA FISH Wash Buffer A (LGC Biosearch Technologies, CA, USA) for 5 min. The probes diluted in deionized formamide Stellaris Hybridization Buffer (LGC Biosearch Technologies, CA, USA) were added to each slide, and incubated overnight at 37 °C in the dark. Unbound probes were removed by incubation with Wash Buffer A for 30 min at 37 °C. And 4′,6-diamidino-2-phenylindole (DAPI) was then applied at 37 °C for 30 min. After removal of DAPI, Wash Buffer B (LGC Biosearch Technologies, CA, USA) was applied to each slide and left for five mins at room temperature. After removal, ~20 μL anti-fade mounting media VECTASHIELD was added and a No.1 coverslip (VWR, UK) was then applied to each sample then sealed using CoverGrip (Biotium, CA, USA). Finally, the samples were imaged with ZEISS Elyra 7 inverted super-resolution microscope. The probes used in this study are listed in Supplementary Table 2.

Quantitative real-time PCR (qRT-PCR)

The RNAs were reverse transcribed with 5×All-In-One MasterMix (ABM, G592). Then qRT-PCR was performed using ChamQ Universal SYBR qPCR Master Mix (Vazyme, Q711-02). The specific primers used in this study are listed in Supplementary Table 2.

Ribo-seq and RNA-seq library construction

Ribo-seq library was constructed as previously described[71]. Briefly, 0.1 g twelve-day-old seedlings powder were lysed with 0.2 mL buffer D (100 mM Tris-HCl (pH 8.0), 40 mM KCl, 20 mM $MgCl_2$, 2% polyoxyethylene (10) tridecyl ether (v/v), 1% deoxycholic acid (w/v), 1 mM DTT, 100 μg/mL cycloheximide, and 10 unit/mL DNase I). The lysate was incubated on ice for 30 min, and then clarified at 13,000 g for 15 min at 4 °C. A 100 μL aliquot of the supernatant was treated with RNase I (Ambion, AM2294) at 23 °C for 1 h, and the reaction was stopped by adding SUPERase•In™ RNase inhibitor (Invitrogen, AM2694). The ribosome-protected fragments were isolated with MicroSpin S-400 HR Columns (GE Healthcare, 27514001). Following RNA isolation and rRNA depletion, the ribosome-protected RNAs (28–32 nt) were separated by a denaturing gel. The Ribo-seq libraries were constructed using NEBNext Multiplex Small RNA Library Prep Set for Illumina (New England Biolabs, E7330). Libraries were pooled for 150 bp paired-end sequencing in a NovaSeq 6000 platform by Annoroad Gene Technology Company in Beijing, China. Another 100 μL aliquot of the supernatant was used to extract total RNA with TRNzol Reagent (TIANGEN, DP405). Total RNA was purified with Dynabeads® mRNA Purification Kit (Invitrogen, 61006). After RNA fragmentation, the RNA was subjected to strand-specific RNA-seq library construction with MGIEasy RNA Directional Library Prep Kit. Sequencing was conducted on the DNBSEQ-T7 platform with 150 bp paired-end reads in The Beijing Genomics Institute (BGI).

Bioinformatics analysis

The bioinformatic analysis was modified from Xu et al.[38]. Adapter sequence was trimmed by Cutadapt[72], then rRNA and tRNA were removed from the ribo-seq reads by Bowtie2[73]. Cleaned reads were mapped to *Arabidopsis* TAIR10 reference genome by Tophat2[74]. Fold changes were calculated using DESeq2[75]. Genes with *FDR* values less than 0.05 and fold change over 1.5 were identified as differentially expressed genes. Genes with RPKM ≥ 1 in Ribo-seq and FPKM ≥ 1 in RNA-seq were kept for the calculation of translational efficiency. The translational efficiency was calculated as the ratio between RPKM in the Ribo-seq and that of FPKM in the RNA-seq, genes with fold change of TE ≥ 1.5 were identified as differentially expressed.

Anthocyanin detection

Twelve-day-old seedlings were ground into powder and lysed in five volumes (5× fresh weight, F.W.) Extraction Buffer (containing 45% methanol and 5% acetic acid). The supernatant was clarified by centrifuging at 13,000 g for 5 min at room temperature for twice. The relative level of anthocyanin was calculated by the absorbance at 530 nm and 657 nm[76].

Statistics & reproducibility

Statistical analysis was performed by GraphPad Prism 8.0. Two groups were analyzed by two-sided unpaired Student's *t*-test. Three or more groups were analyzed by One-way ANOVA with Dunnett's multiple comparisons test. Data was presented as mean values ± SD. P value < 0.05 was considered as significant difference. No data was excluded from the analyses. Details of the biological replicates were provided in figure legends wherever necessary.

Reporting summary

Further information on research design is available in the Nature Portfolio Reporting Summary linked to this article.

Data availability

The sequencing data have been deposited in the Genome Sequence Archive in National Genomics Data Center, Beijing Institute of Genomics, Chinese Academy of Sciences under accession code CRA013783. The mass spectrometry proteomics data have been deposited in the ProteomeXchange Consortium via the iProX partner repository with the dataset identifier PXD055607 and PXD055608 (http://proteomecentral.proteomexchange.org/cgi/GetDataset?ID=PXD055607; http://proteomecentral.proteomexchange.org/cgi/GetDataset?ID=PXD055608). Source data are provided with this paper.

References

1. Hu, Y. et al. Molecular mechanisms of adaptive evolution in wild animals and plants. *Sci. China Life Sci.* **66**, 453–495 (2023).
2. Gong, Z. et al. Plant abiotic stress response and nutrient use efficiency. *Sci. China Life Sci.* **63**, 635–674 (2020).
3. Thomashow, M. F. PLANT COLD ACCLIMATION: freezing tolerance genes and regulatory mechanisms. *Annu. Rev. Plant Physiol. Plant Mol. Biol.* **50**, 571–599 (1999).
4. Ding, Y., Shi, Y. & Yang, S. Molecular regulation of plant responses to environmental temperatures. *Mol. Plant* **13**, 544–564 (2020).
5. Woolford, J. L. Jr. & Baserga, S. J. Ribosome biogenesis in the yeast *Saccharomyces cerevisiae*. *Genetics* **195**, 643–681 (2013).
6. Saez-Vasquez, J. & Delseny, M. Ribosome biogenesis in plants: from functional 45S ribosomal DNA organization to ribosome assembly factors. *Plant Cell* **31**, 1945–1967 (2019).
7. Weis, B. L., Kovacevic, J., Missbach, S. & Schleiff, E. Plant-specific features of ribosome biogenesis. *Trends Plant Sci* **20**, 729–740 (2015).
8. Dorner, K., Ruggeri, C., Zemp, I. & Kutay, U. Ribosome biogenesis factors-from names to functions. *EMBO J* **42**, e112699 (2023).
9. Munoz-Diaz, E. & Saez-Vasquez, J. Nuclear dynamics: Formation of bodies and trafficking in plant nuclei. *Front. Plant Sci.* **13**, 984163 (2022).
10. Li, X. & Gu, Y. Structural and functional insight into the nuclear pore complex and nuclear transport receptors in plant stress signaling. *Curr. Opin. Plant Biol.* **58**, 60–68 (2020).
11. Yang, Y., Wang, W., Chu, Z., Zhu, J. K. & Zhang, H. Roles of nuclear pores and nucleo-cytoplasmic trafficking in plant stress responses. *Front. Plant Sci.* **8**, 574 (2017).
12. Zhang, A. et al. Nuclear pore complex components have temperature-influenced roles in plant growth and immunity. *Plant Cell Environ* **43**, 1452–1466 (2020).
13. Merchante, C., Stepanova, A. N. & Alonso, J. M. Translation regulation in plants: an interesting past, an exciting present and a promising future. *Plant J* **90**, 628–653 (2017).
14. Shanmugam, T. et al. An Arabidopsis divergent pumilio protein, APUM24, is essential for embryogenesis and required for faithful pre-rRNA processing. *Plant J* **92**, 1092–1105 (2017).
15. Maekawa, S., Ishida, T. & Yanagisawa, S. Reduced expression of APUM24, encoding a novel rRNA processing factor, induces sugar-dependent nucleolar stress and altered sugar responses in *Arabidopsis thaliana*. *Plant Cell* **30**, 209–227 (2017).
16. Zu, X. et al. A mitochondrial pentatricopeptide repeat protein enhances cold tolerance by modulating mitochondrial superoxide in rice. *Nat. Commun.* **14**, 6789 (2023).
17. Wang, Z. et al. Pseudouridylation of chloroplast ribosomal RNA contributes to low temperature acclimation in rice. *New Phytol* **236**, 1708–1720 (2022).
18. Xu, T. et al. A ZTF-7/RPS-2 complex mediates the cold-warm response in *C. elegans*. *PLOS Genetics* **19**, e1010628 (2023).
19. de la Cruz, J. et al. Feedback regulation of ribosome assembly. *Curr. Genet.* **64**, 393–404 (2018).
20. Zhang, H., Zhao, Y. & Zhu, J. K. Thriving under stress: how plants balance growth and the stress response. *Dev. Cell* **55**, 529–543 (2020).
21. Iserman, C. et al. Condensation of ded1p promotes a translational switch from housekeeping to stress protein production. *Cell* **181**, 818–831.e19 (2020).
22. Chantarachot, T. et al. DHH1/DDX6-like RNA helicases maintain ephemeral half-lives of stress-response mRNAs. *Nat. Plants* **6**, 675–685 (2020).
23. Hang, R. et al. *Arabidopsis* protein arginine methyltransferase 3 is required for ribosome biogenesis by affecting precursor ribosomal RNA processing. *Proc. Natl. Acad. Sci. USA* **111**, 16190–16195 (2014).
24. Hang, R. et al. Protein arginine methyltransferase 3 fine-tunes the assembly/disassembly of pre-ribosomes to repress nucleolar stress by interacting with RPS2B in *Arabidopsis*. *Mol. Plant* **14**, 223–236 (2021).
25. Watkins, N. J. & Bohnsack, M. T. The box C/D and H/ACA snoRNPs: key players in the modification, processing and the dynamic folding of ribosomal RNA. *Wiley Interdiscip. Rev. RNA* **3**, 397–414 (2012).
26. Lin, D. H. & Hoelz, A. The structure of the nuclear pore complex (An update). *Annu. Rev. Biochem.* **88**, 725–783 (2019).
27. Tingey, M., Li, Y., Yu, W., Young, A. & Yang, W. Spelling out the roles of individual nucleoporins in nuclear export of mRNA. *Nucleus* **13**, 170–193 (2022).
28. Stade, K., Ford, C. S., Guthrie, C. & Weis, K. Exportin 1 (Crm1p) is an essential nuclear export factor. *Cell* **90**, 1041–1050 (1997).
29. Thomas, F. & Kutay, U. Biogenesis and nuclear export of ribosomal subunits in higher eukaryotes depend on the CRM1 export pathway. *J. Cell Sci.* **116**, 2409–2419 (2003).
30. Kudo, N. et al. Leptomycin B inactivates CRM1/exportin 1 by covalent modification at a cysteine residue in the central conserved region. *Proc. Natl. Acad. Sci. USA* **96**, 9112–9117 (1999).
31. Blanvillain, R., Boavida, L. C., McCormick, S. & Ow, D. W. Exportin1 genes are essential for development and function of the gametophytes in *Arabidopsis thaliana*. *Genetics* **180**, 1493–1500 (2008).
32. Tamura, K., Fukao, Y., Iwamoto, M., Haraguchi, T. & Hara-Nishimura, I. Identification and characterization of nuclear pore complex components in *Arabidopsis thaliana*. *Plant Cell* **22**, 4084–4097 (2010).
33. Li, C., Liu, L., Teo, Z. W. N., Shen, L. & Yu, H. Nucleoporin 160 regulates flowering through anchoring HOS1 for destabilizing CO in *Arabidopsis*. *Plant Commun* **1**, 100033 (2020).
34. Cheng, Z. et al. Nup96 and HOS1 are mutually stabilized and gate constans protein level, conferring long-day photoperiodic flowering regulation in *Arabidopsis*. *Plant Cell* **32**, 374–391 (2020).
35. Kilian, J. et al. The AtGenExpress global stress expression data set: protocols, evaluation and model data analysis of UV-B light, drought and cold stress responses. *Plant J* **50**, 347–363 (2007).
36. Ingolia, N. T., Ghaemmaghami, S., Newman, J. R. & Weissman, J. S. Genome-wide analysis in vivo of translation with nucleotide resolution using ribosome profiling. *Science* **324**, 218–223 (2009).
37. Merchante, C. et al. Gene-specific translation regulation mediated by the hormone-signaling molecule EIN2. *Cell* **163**, 684–697 (2015).
38. Xu, G. et al. Global translational reprogramming is a fundamental layer of immune regulation in plants. *Nature* **545**, 487–490 (2017).
39. Dong, N. Q. & Lin, H. X. Contribution of phenylpropanoid metabolism to plant development and plant-environment interactions. *J. Integr. Plant Biol.* **63**, 180–209 (2021).
40. Schulz, E., Tohge, T., Zuther, E., Fernie, A. R. & Hincha, D. K. Flavonoids are determinants of freezing tolerance and cold acclimation in *Arabidopsis thaliana*. *Sci. Rep.* **6**, 34027 (2016).
41. Li, P. et al. The Arabidopsis UDP-glycosyltransferases UGT79B2 and UGT79B3, contribute to cold, salt and drought stress tolerance via modulating anthocyanin accumulation. *Plant J* **89**, 85–103 (2017).
42. Lafontaine, D. L. J., Riback, J. A., Bascetin, R. & Brangwynne, C. P. The nucleolus as a multiphase liquid condensate. *Nat. Rev. Mol. Cell Biol.* **22**, 165–182 (2021).
43. Boulon, S., Westman, B. J., Hutten, S., Boisvert, F. M. & Lamond, A. I. The nucleolus under stress. *Mol. Cell* **40**, 216–227 (2010).
44. Black, J. J., Musalgaonkar, S. & Johnson, A. W. Tsr4 Is a Cytoplasmic Chaperone for the Ribosomal Protein Rps2 in *Saccharomyces cerevisiae*. *Mol. Cell. Biol.* **39**, e00094–19 (2019).
45. Landry-Voyer, A. M., Bergeron, D., Yague-Sanz, C., Baker, B. & Bachand, F. PDCD2 functions as an evolutionarily conserved chaperone dedicated for the 40S ribosomal protein uS5 (RPS2). *Nucleic Acids Res* .**48**, 12900–12916 (2020).

46. Landry-Voyer, A. M. et al. Human PDCD2L Is an export substrate of CRM1 that associates with 40S ribosomal subunit precursors. *Mol. Cell Biol.* **36**, 3019–3032 (2016).
47. Dong, C. H., Agarwal, M., Zhang, Y., Xie, Q. & Zhu, J. K. The negative regulator of plant cold responses, HOS1, is a RING E3 ligase that mediates the ubiquitination and degradation of ICE1. *Proc. Natl. Acad. Sci. USA* **103**, 8281–8286 (2006).
48. Gong, Z. et al. A DEAD box RNA helicase is essential for mRNA export and important for development and stress responses in *Arabidopsis*. *Plant Cell* **17**, 256–267 (2005).
49. Jia, Y. et al. The cbfs triple mutants reveal the essential functions of CBFs in cold acclimation and allow the definition of CBF regulons in *Arabidopsis*. *New Phytol* **212**, 345–353 (2016).
50. Zhao, C. et al. Mutational evidence for the critical role of CBF transcription factors in cold acclimation in *Arabidopsis*. *Plant Physiol* **171**, 2744–2759 (2016).
51. Olate, E., Jimenez-Gomez, J. M., Holuigue, L. & Salinas, J. NPR1 mediates a novel regulatory pathway in cold acclimation by interacting with HSFA1 factors. *Nat. Plants* **4**, 811–823 (2018).
52. Li, H. et al. BZR1 positively regulates freezing tolerance via CBF-dependent and CBF-independent pathways in *Arabidopsis*. *Mol. Plant* **10**, 545–559 (2017).
53. VanBogelen, R. A. & Neidhardt, F. C. Ribosomes as sensors of heat and cold shock in *Escherichia coli*. *Proc. Natl. Acad. Sci. USA* **87**, 5589–5593 (1990).
54. Hang, R. et al. Ribosomal RNA biogenesis and its response to chilling stress in *Oryza sativa*. *Plant Physiol* **177**, 381–397 (2018).
55. Garcia-Molina, A. et al. Translational components contribute to acclimation responses to high light, heat, and cold in *Arabidopsis*. *iScience* **23**, 101331 (2020).
56. Liu, H. et al. HsfA1d promotes hypocotyl elongation under chilling via enhancing expression of ribosomal protein genes in *Arabidopsis*. *New Phytol* **231**, 646–660 (2021).
57. Cheong, B. E. et al. Arabidopsis REI-LIKE proteins activate ribosome biogenesis during cold acclimation. *Sci. Rep.* **11**, 2410 (2021).
58. Yu, H. et al. STCH4/REIL2 confers cold stress tolerance in *Arabidopsis* by promoting rRNA processing and CBF protein translation. *Cell Reports* **30**, 229–242 (2020).
59. Shi, Z. & Barna, M. Translating the genome in time and space: specialized ribosomes, RNA regulons, and RNA-binding proteins. *Annu. Rev. Cell Dev. Biol.* **31**, 31–54 (2015).
60. Martinez-Seidel, F., Beine-Golovchuk, O., Hsieh, Y. C. & Kopka, J. Systematic review of plant ribosome heterogeneity and specialization. *Front. Plant Sci.* **11**, 948 (2020).
61. Shi, Z. et al. Heterogeneous ribosomes preferentially translate distinct subpools of mRNAs genome-wide. *Mol. Cell* **67**, 71–83.e7 (2017).
62. Wu, H.-Y. L., Jen, J. & Hsu, P. Y. What, where, and how: regulation of translation and the translational landscape in plants. *Plant Cell* **36**, 1540–1564 (2023).
63. Leppek, K., Das, R. & Barna, M. Functional 5′ UTR mRNA structures in eukaryotic translation regulation and how to find them. *Nat. Rev. Mol. Cell Biol.* **19**, 158–174 (2018).
64. Xu, G. et al. uORF-mediated translation allows engineered plant disease resistance without fitness costs. *Nature* **545**, 491–494 (2017).
65. Tsutsui, H. & Higashiyama, T. pKAMA-ITACHI vectors for highly efficient CRISPR/Cas9-mediated gene knockout in *Arabidopsis thaliana*. *Plant Cell Physiol* **58**, 46–56 (2017).
66. Yan, W. et al. Simultaneous Identification of Multiple Causal Mutations in Rice. *Front. Plant Sci.* **7**, 2055 (2017).
67. Mustroph, A., Juntawong, P. & Bailey-Serres, J. Isolation of plant polysomal mRNA by differential centrifugation and ribosome immunopurification methods. *Methods Mol. Biol.* **553**, 109–126 (2009).
68. Chen, H. et al. Firefly luciferase complementation imaging assay for protein-protein interactions in plants. *Plant Physiol* **146**, 368–376 (2008).
69. Waadt, R. et al. Multicolor bimolecular fluorescence complementation reveals simultaneous formation of alternative CBL/CIPK complexes in planta. *Plant J* **56**, 505–516 (2008).
70. Duncan, S., Johansson, H. E. & Ding, Y. Reference genes for quantitative Arabidopsis single molecule RNA fluorescence in situ hybridization. *J. Exp. Bot.* **74**, 2405–2415 (2023).
71. Hsu, P. Y. et al. Super-resolution ribosome profiling reveals unannotated translation events in *Arabidopsis*. *Proc. Natl. Acad. Sci. USA* **113**, E7126–E7135 (2016).
72. Martin, M. Cutadapt removes adapter sequences from high-throughput sequencing reads. *EMBnet. J.* **17**, 10–12 (2011).
73. Langmead, B. & Salzberg, S. L. Fast gapped-read alignment with Bowtie 2. *Nat. Methods* **9**, 357–359 (2012).
74. Kim, D. et al. TopHat2: accurate alignment of transcriptomes in the presence of insertions, deletions and gene fusions. *Genome Biol* **14**, R36 (2013).
75. Love, M. I., Huber, W. & Anders, S. Moderated estimation of fold change and dispersion for RNA-seq data with DESeq2. *Genome Biol* **15**, 550 (2014).
76. Nakata, M. & Ohme-Takagi, M. Quantification of anthocyanin content. *Bio-protocol* **4**, e1098 (2014).

Acknowledgements

We thank Jifeng Wang at Laboratory of Proteomics, Institute of Biophysics, Chinese Academy of Sciences for assistance in mass spectrometry, and John Innes Centre Bioimaging facility for support. We thank Yongfu Fu at Chinese Academy of Agricultural Sciences for sharing *hos1-3* mutants, and Shuhua Yang at China Agricultural University for sharing the *cbfs* mutants. We thank Hui Li for help in freezing treatment assays. This work was supported by grants from the National Key Research and Development Program (2020YFA0509903 to X.C.), National Natural Science Foundation of China (32100424, and 32241038 to Z.W., and 32171284 to C.L.), the Chinese Academy of Sciences (Strategic Priority Research Program XDB27030201 to X.C.).

Author contributions

X.C. and Z.W. conceived and designed the experiment; Z.W. and X.Z. performed most of the experiments; Z.W. performed Ribo-seq library construction with help from C.L.; X.Z. performed bioinformatics analysis with help from J.S.; S.D. performed RNA-FISH; R.H., L.L., and Y.D. commented on the manuscript. Z.W., X.Z., and X.C. wrote the paper.

Competing interests

The authors declare no competing interests.

Additional information

Supplementary information The online version contains supplementary material available at https://doi.org/10.1038/s41467-024-52945-8.

Correspondence and requests for materials should be addressed to Zhen Wang or Xiaofeng Cao.

Peer review information *Nature Communications* thanks the anonymous reviewers for their contribution to the peer review of this work. A peer review file is available.